Oxidation Behavior of TD-NiCr in a Dynamic High Temperature Environment

D. R. TENNEY, C. T. YOUNG, AND H. W. HERRING

The oxidation behavior of TD-NiCr has been studied in static and high-speed flowing air environments at 1100 and 1200°C. The surface oxide topographies and microstructures formed in both types of environments have been characterized and compared to explain some of the observed differences in the oxidation behavior for the two types of tests. It has been found that the stable oxide morphologies formed on the specimens exposed to the static and dynamic environments were markedly different. The faceted crystal morphology characteristic of static oxidation was found to be unstable under high-temperature, high-speed flow conditions and was quickly replaced by a porous NiO "mushroom" type structure. Also, it was found that the rate of formation of CrO_3(v) from Cr_2O_3(s) was greatly enhanced by high gas velocity conditions. The stability of Cr_2O_3 was found to be greatly improved by the presence of an outer NiO layer, even though the NiO layer was very porous. An oxidation model is proposed to explain the observed microstructures and overall oxidation behavior of TD-NiCr alloys.

RECENT interest in high temperature, high-strength alloys for such potential applications as used in advanced jet engines and as part of the thermal protection system for space shuttle, has focused attention on dispersion-strengthened nickel-base alloys. One such alloy which has received much consideration because of its combination of good oxidation resistance and good high temperature strength, is Ni-20 Cr-2 ThO_2 supplied under the trade name TD-NiCr. The oxidation resistance of this alloy in the 900 to 1200°C temperature range under static furnace atmosphere conditions has been studied by a number of different investigators.[1-16] It is well established that the oxidation resistance of this alloy is due to the formation of a protective Cr_2O_3 layer on the surface which has excellent adherence to the substrate. However, it has also been shown that, for temperatures above about 1040°C the Cr_2O_3 layer is subject to significant weight loss because of the formation of a volatile CrO_3 oxide phase. Giggins and Pettit[4] and more recently Stringer[12] have proposed analyses based on the work of Tedmon[17] to correct weight gain data to account for this weight loss. The overall rate of metal consumption is, to a large part, determined by an interplay between the rate of scale thickening due to oxidation and the rate of scale thickness decrease due to the formation and volatization of CrO_3. Oxide vaporization which may not be severe in static or slowly moving gas environments may be excessive under high speed flowing air conditions where volatile oxide species are rapidly swept away by the gas stream. A high vaporization rate tends to reduce the protective oxide thickness, and hence increases the rate of metal consumption. It is therefore clear that to establish reliability of flight weight, metallic heat shields for the thermal protection system of space shuttle, tests must be conducted under shuttle re-entry conditions. Such tests have been conducted at several NASA Centers[18-24] using arc-jet tests to simulate re-entry conditions.

These studies have clearly demonstrated that TD-NiCr does oxidize more rapidly in simulated re-entry tests than in similar static furnace tests. Centolanzi[23] presents data for TD-NiCr which show that, for arc-jet tests conducted in flowing air, 15 torr total pressure, and 1200°C for 50 one-half h cycles, the average metal loss was roughly 0.051 mm. Using the weight gain data of Giggins and Pettit[4] for static oxidation at 1200°C in 0.1 atm O_2 and correcting for vaporization losses, a calculation of substrate thickness decrease shows that 0.0026 mm of alloy should be oxidized in 25 h. A comparison of these two numbers reveals that there is approximately a twenty-fold increase or more than an order of magnitude increase in the rate of substrate thickness decrease in the high speed flowing air tests. Likewise, Lowell and Sanders[22] at NASA Lewis Research Center have exposed TD-NiCr to a Mach-1, 1-atmosphere jet A-1 fuel gas stream at 1200°C for times to 50 h. They observed that nearly 100 times as much metal was lost in their high gas-velocity test as in static tests.

Arc-jet tests conducted at NASA-Langley Research Center by the authors support the above findings that high speed gas flow over the specimen increases the overall rate of oxidation of the alloy. Careful metallographic analyses of the oxide layers formed on arc-jet tested specimens have revealed oxide morphology changes not previously reported. It was found that the outer oxide scale was a porous "mushroom" type NiO layer, representing a morphology totally different from that observed for specimens oxidized in static air. Since the presence of this layer should have a direct influence on the observed oxidation behavior of this alloy, a detailed study was undertaken to characterize the oxide scale morphology, composition, and microstructure formed on TD-NiCr under simulated re-entry conditions. It was planned that the basic information collected from this study would be combined with that reported for static and other dynamic tests to develop an oxidation model to explain the overall

D. R. TENNEY is Assistant Professor of Metallurgical Engineering, Div. of Minerals Engineering, Virginia Polytechnic Institute and State University, Blacksburg, Va. 24061. C. T. YOUNG, formerly a Research Fellow at Langley Research Center, Hampton, Va., is now with Bendix Research Center, Bendix Corp., Southfield, Mich. 48076. H. W. HERRING is a Materials Engineer, NASA-Langley Research Center, Hampton, Va. 23365.

Manuscript submitted August 22, 1973.

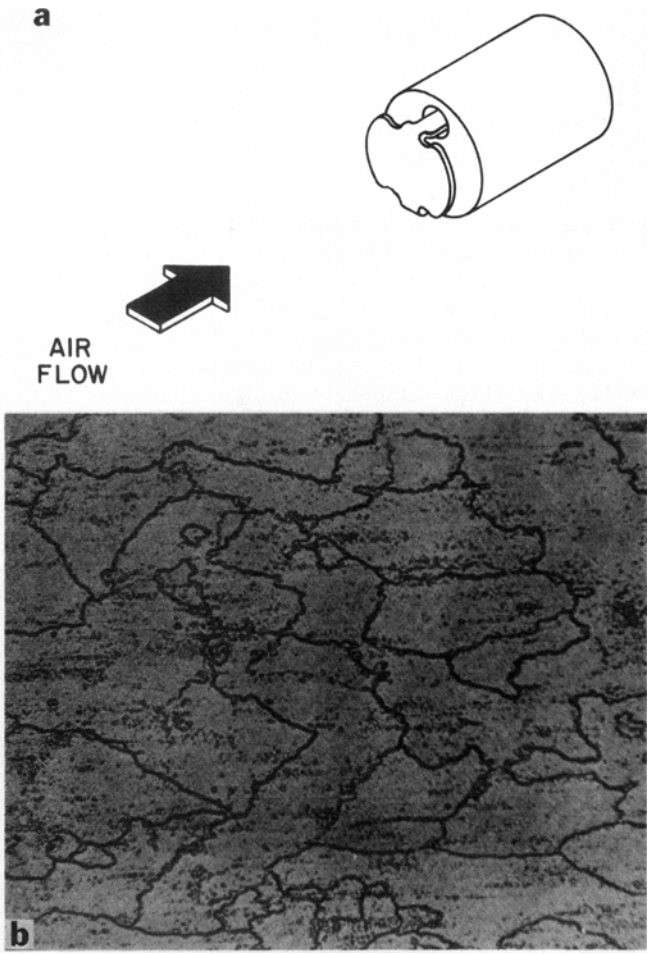

Fig. 1—(*a*) Schematic of TD-NiCr specimen mounted in arc-jet specimen holder. (*b*) Micrograph of alloy grain structure of as-received TD-NiCr.

oxidation behavior of this alloy. To this end, experiments were undertaken to reveal the effects of temperature and mass flow rate on the dynamic oxidation behavior. Using the data thus collected, a model of the oxidation process for simulated re-entry conditions has been developed to explain the observed oxide microstructures.

EXPERIMENTAL PROCEDURE

Materials and Preparation

The alloy Ni-20 Cr-2 ThO_2 supplied under the trade name of TD-NiCr used in this study was produced by Fansteel, Inc. by a combination of powder metallurgy techniques and thermomechanical treatments and was delivered in a recrystallized condition with a belt-sanded surface finish. Specimens were punched from 0.020 inch sheet and had a 5/16 in. by 7/32 in. oblong shape test surface with two legs extended in the direction along the short axis. The legs were bent to give the configuration which fit to the arc-jet specimen holder as shown in Fig. 1(*a*).

To examine the grain structure of the as-received alloy, the specimens were metallographically polished through 6 μm diamond paste and electropolished for one minute in a solution of 87 ml methanol, 8 ml H_2SO_4, 3 ml HNO_3, and 2 ml HF at room temperature and 17 volts. They were then oxidized in air at 1100 to 1200°C for 15 to 20 sec. Grain patterns were clearly brought out due to the preferential formation of Cr_2O_3 at grain boundaries and NiO within grains. Grain structure was also examined by etching the sample electrolitically in a solution of 10 pct oxalic acid at room temperature and 5 volts for 20 sec. Typical microstructure of the alloy is shown in Fig. 1(*b*). The matrix grains were thin in the sheet thickness direction and somewhat elongated in the rolling direction. The grain boundaries were jagged and irregular. Stringers of Cr_2O_3 particles which formed during processing were observed parallel to the rolling direction. X-ray diffraction analysis indicated that the alloy has a very strong preferred orientation with the {100} planes aligned parallel to the sheet surface.

Arc-Heater Testing Equipment

The equipment used for the dynamic oxidation tests was an Aerotherm 100 kw constrictor arc-heater system designed to give convective heating conditions similar to hypersonic flight. This equipment is located at NASA-Langley Research Center and is described in detail in Ref. 25. The test chamber contains a pneumatically driven model support system so arranged to allow the specimen to be inserted into the stream by translating radially inward. The positioning of this system is such that the specimens were inserted into the jet stream approximately 6 in. downstream of the nozzle where lamellar flow conditions existed. The specimens were inserted into the stream in a stagnation geometry with the surface of the test specimen perpendicular to the direction of flow of the gas stream. With this configuration, a boundary layer is present on the specimen surface, except at the extreme edges where high speed flow conditions exist. The thickness of this boundary layer for the type of tests being conducted in this investigation was calculated by Aerotherm Corporation (manufacturer of the arc-jet used) to be on the order of magnitude of 360 μm. Viewing ports with pyrex glass windows and pyrometer ports with optical grade quartz were located on both sides of the test chamber to permit observation of the specimen during testing. The temperature of the test specimen was determined either with a calibrated optical pyrometer or with a thermocouple attached to the back of the specimen.

Specimens were oxidized in the arc-heater system under the condition of 1200°C, Mach-5 air stream velocity, 0.002 lbs/sec mass flow rate, 1916 BTU/lb stream enthalpy, 12.74 BTU/ft^2-sec cold-wall heating rate, and a stagnation pressure of 5 torr. A limited number of tests were also conducted at a mass flow rate of 0.008 lbs/sec, which gave a stagnation pressure of 17 torr and a stream enthalpy of 1368 BTU/lb. To study the effect of temperature selected tests were also performed at 1100°C at the two mass flow rates used at 1200°C. The exposure times examined for the 1200°C and 0.002 $\dot{m}$ conditions were 15 sec, 30 sec, 1 min, 10 min, 30 min, 2 h, 5 h, 10 h, 16 h, and 20 h. All tests for exposure times longer than 30 min were cyclic tests wherein the specimen was exposed for 30 min, cooled in static air, then recycled until the desired time at temperature had been accumulated. The starting surface condition of all specimens was main-

Table I. Oxides Determined by X-ray Diffraction on TD-NiCr Preoxidized in Air at 1100°C for 1 h and Isothermally Exposed at 1200°C in High-Gas Velocity Apparatus for Various Times

Exposure Time	Alloy Substrate		Surface Oxides									
			ThO_2				Cr_2O_3			NiO		
	(111)	(200)	(111)	(200)	(220)	(311)	(012)	(104)	(110)	(111)	(200)	(220)
As-P.O.	*S*	*VS*	*M*	*W*	*W*	*W*	*W*	*M*				
15 sec	*M*	*VS*	*W*	*VW*	*VW*	*VW*	*VW*					
30 sec	*M*	*S*	*W*	*VW*	*VW*	*VW*	*VW*			*M*	*M*	*W*
1 min	*W*	*VS*	*W*				*VW*	*W*		*S*	*S*	*S*
3 min	*VW*	*VS*	*W*				*VW*	*W*		*S*	*S*	*S*
10 min	*VW*	*VS*	*VW*				*VW*	*VW*		*S*	*VS*	*S*
30 min	*VW*	*VS*	*W*				*VW*	*W*	*VW*	*S*	*S*	*M*
2 h		*VS*	*M*	*W*	*W*	*W*	*W*	*W*	*VW*	*M*	*M*	*W*
10 h		*VS*	*S*		*M*	*M*	*W*	*W*	*VW*	*M*	*M*	*M*

VS = Very Strong; *S* = Strong; *M* = Medium; *W* = Weak; *VW* = Very Weak. Blank = Reflection Not Detected.

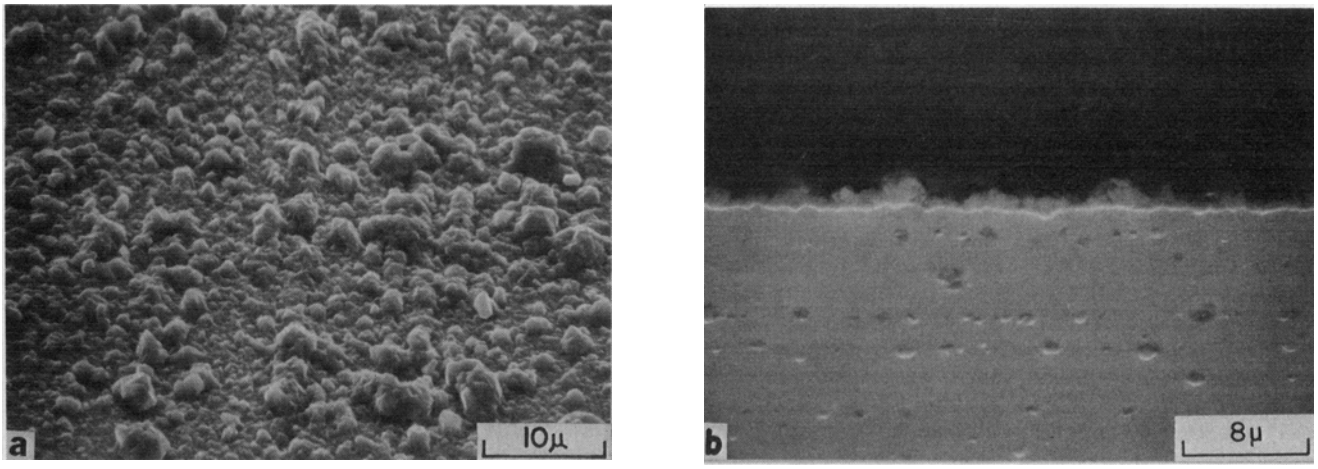

Fig. 2—Surface oxide scale formed on TD-NiCr. (*a*) Topography, showing generally fine grained oxide formed after 1 h at 1100°C in static air. (*b*) Showing the oxide/alloy cross-section.

tained constant by preoxidizing the as-received (belt sanded finish) specimens at 1100°C for 1 h in air before arc-jet testing. The purpose of this preoxidation treatment was to form an oxide layer that provided a high emissivity surface, a condition desired for the material to be used as a thermal protection heat shield.

Analysis of Oxide Layers

Conventional metallographic, X-ray diffraction, and scanning electron microscopy were employed to characterize the oxide scale on both statically and dynamically tested specimens. The X-ray diffraction studies were made using vanadium filtered chromium radiation on the oxides *in situ* and on spalled oxides. The diffraction patterns were evaluated mainly by using the standard ASTM Powder Diffraction Index. A summary of the X-ray analysis results are given in Table I. Qualitative chemical analysis of the oxides observed in the scanning microscope was carried out using a Nuclear Diodes energy dispersive X-ray analysis system (EDAX). The oxidized specimens, after observation of surface oxide morphology, were carefully cut into halves. One half was bent to break away part of the oxide layer from the metal substrate. The oxide morphology and oxide chemical composition were again studied. The other half was mounted in epoxy for metallographic observation, substrate thickness decrease measurements, and electron microprobe analysis. The probe analysis was carried out using an ARL electron microprobe operated at 15 kV and 0.05 μamp beam current. MAGIC computer program developed by Colby[26] was used to correct the raw data.

To determine the amount of alloy substrate oxidized as a function of exposure time in the arc-jet substrate thickness measurements were made before and after testing. The procedure was to measure the thickness of the specimens before testings with a Cortex micrometer found to be accurate to ±0.0001 inch. Measurements were made at five different areas on the surface, and only those specimens found to be of uniform thickness were used. After oxidation, the specimens were sectioned and polished such that the cross-sectional thickness of the specimen could be measured optically using a calibrated vernier eye piece.

EXPERIMENTAL RESULTS

The morphology and cross-section of the oxide scale formed on TD-NiCr specimens with as-received surface finish (belt sanded) after static oxidation in air at 1100°C for one hour are shown in Fig. 2. The faceted granular surface oxide was identified by X-ray diffraction to be Cr_2O_3 consistent with the results of other investigators that only Cr_2O_3 forms on specimens with a mechanically polished surface finish. The selective

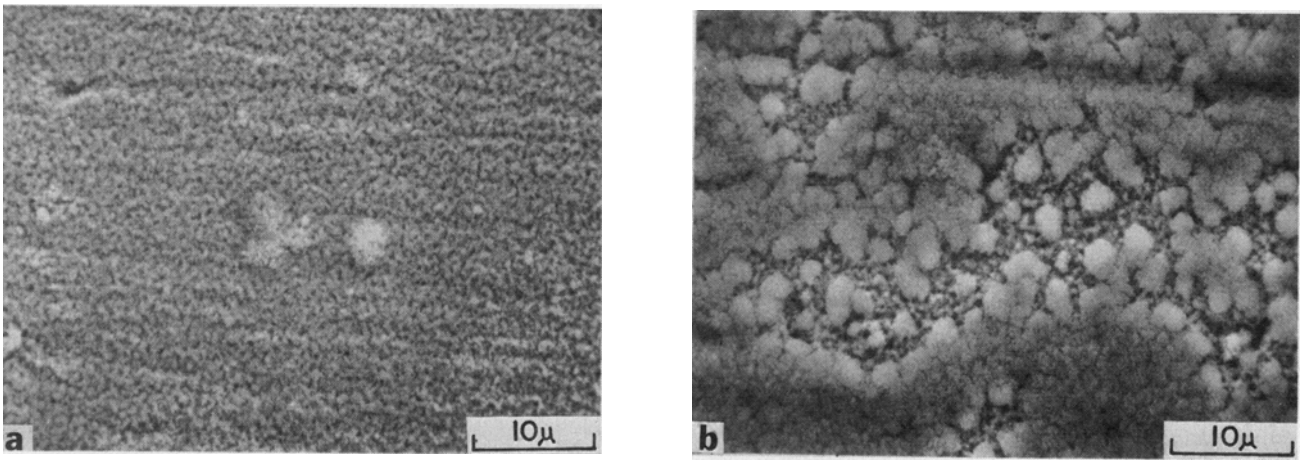

Fig. 3—Surface oxide topographies formed on TD-NiCr exposed at 1200°C in mach-5 arc-jet for times of (*a*) 15 sec and (*b*) 30 sec.

oxidation of chromium is generally believed[11] to result from the preferential nucleation of Cr_2O_3 at ThO_2 particles on the surface and enhanced diffusion of Cr to the surface along numerous grain boundaries in a thin recrystallized surface layer. The presence of a thin (approximately 2 μm) recrystallized layer in the alloy adjacent to the oxide was experimentally observed on polished and etched cross-sections of oxidized specimens with a belt-sanded surface finish and on specimens polished through 600 grit polishing paper. Although the recrystallized layer was much thinner on the specimens with the 600 grit finish as compared with the belt-sanded, the Cr_2O_3 oxide layers appeared nearly identical. On both types of specimens, the Cr_2O_3 layer was always continuous and approximately 1 μm in thickness. Electron microprobe scans of polished cross-sections indicated the existence of a small Cr depletion zone in the alloy adjacent to the oxide. X-ray diffraction patterns of the preoxidized as-received specimens contained the {111} and {200} alloy reflections and identifiable peaks for the ThO_2 and Cr_2O_3 oxide phases. The {111} alloy peak was primarily produced by the recrystallized surface layer which formed during the early stage of static oxidation. This statement is based on the fact that the {111} reflection was never detected from the as-received specimens, presumably because of the strong {200} preferred orientation of the TD-NiCr sheet from which the specimens were prepared.

Micrographs illustrating the topologies of surface oxides developed on specimens dynamically tested at 1200°C in a Mach-5 arc-jet for times of 15 sec and 30 sec are presented in Fig. 3. Normally, it took about 10 to 12 sec to heat the specimen to 1200°C in the arc-heater furnace. In Fig. 3 it is seen that after only 15 sec oxidation, the solid granular Cr_2O_3 oxide scale on the surface (from the preoxidation treatment) has been changed to a very porous oxide layer. Only one very weak Cr_2O_3 reflection, and no reflections of NiO, were observed in X-ray analysis, suggesting that the original Cr_2O_3 oxide either spalled or nearly all vaporized. The fact that Cr_2O_3 is known to have excellent adherence to the alloy indicated that the loss of Cr_2O_3 due to spalling is unlikely. No evidence for spalling at any area on the surface could be found in either low magnification or high magnification scanning micrographs made of the surface. It is therefore concluded that the absence of Cr_2O_3 is due to vaporization through the formation of volatile CrO_3. The thin porous oxide observed is presumably the remains of the original Cr_2O_3 layer. It has been reported that the atomic oxygen which exists in high temperature, high-velocity, flowing air can greatly enhance the following reactions; $Cr_2O_3 + 3O \rightarrow 2CrO_3$ and $Ni + O \rightarrow NiO$.[27,30] It is believed that in the dynamic tests conducted in the present study, a small but significant fraction of the molecular oxygen in the stream is dissociated into atomic oxygen.[31] Although the amount of dissociation is not known, there appears to be a sufficient supply of atomic oxygen to greatly accelerate the rate of formation of CrO_3 which is rapidly swept away by the gas stream, thus leading to nearly total loss of the original Cr_2O_3 layer in 15 sec of exposure. Hagel[32] has reported that for the reaction of Cr_2O_3 with oxygen at 0.1 atm, the volatilization rate constant for the loss of Cr_2O_3 via CrO_3 formation is given by

$$K_v = 0.214 \exp(-48{,}000 \pm 3000/RT) \text{ (gr/cm}^2\text{·sec)}$$

Considering a unit cross-sectional area and taking the density of Cr_2O_3 as 5.21 gr/cm^3, it can readily be shown that 3.24×10^{-5} μm of Cr_2O_3 would be lost per sec. At this rate of loss, it would take approximately 8.6 h to remove 1 μm of Cr_2O_3. Although the test conditions in the arc-jet are quite different from those for which Hagel's data apply, this calculation does serve to point out the tremendous acceleration in the rate of volatilization of Cr_2O_3 in the arc-jet environment.

The surface oxide topography formed after 30 sec of oxidation in the arc-jet is shown in Fig. 3(*b*). Most of the surface is covered with a porous oxide matt. On the more open areas of the surface, oxide clusters in the shape of "mushrooms" are seen to form on top of a porous substrate, presumably the remains of the original Cr_2O_3 layer. Both the oxide matt and the "mushroom" type oxide were identified to be NiO.

Fig. 4 shows the surface and oxide cross-section of a specimen after 1 minute of exposure. Most of the surface is now covered with "mushroom" type NiO formations. High magnification micrographs indicate that the mushroom type oxide formations are very porous and consist of a cluster of numerous fine NiO

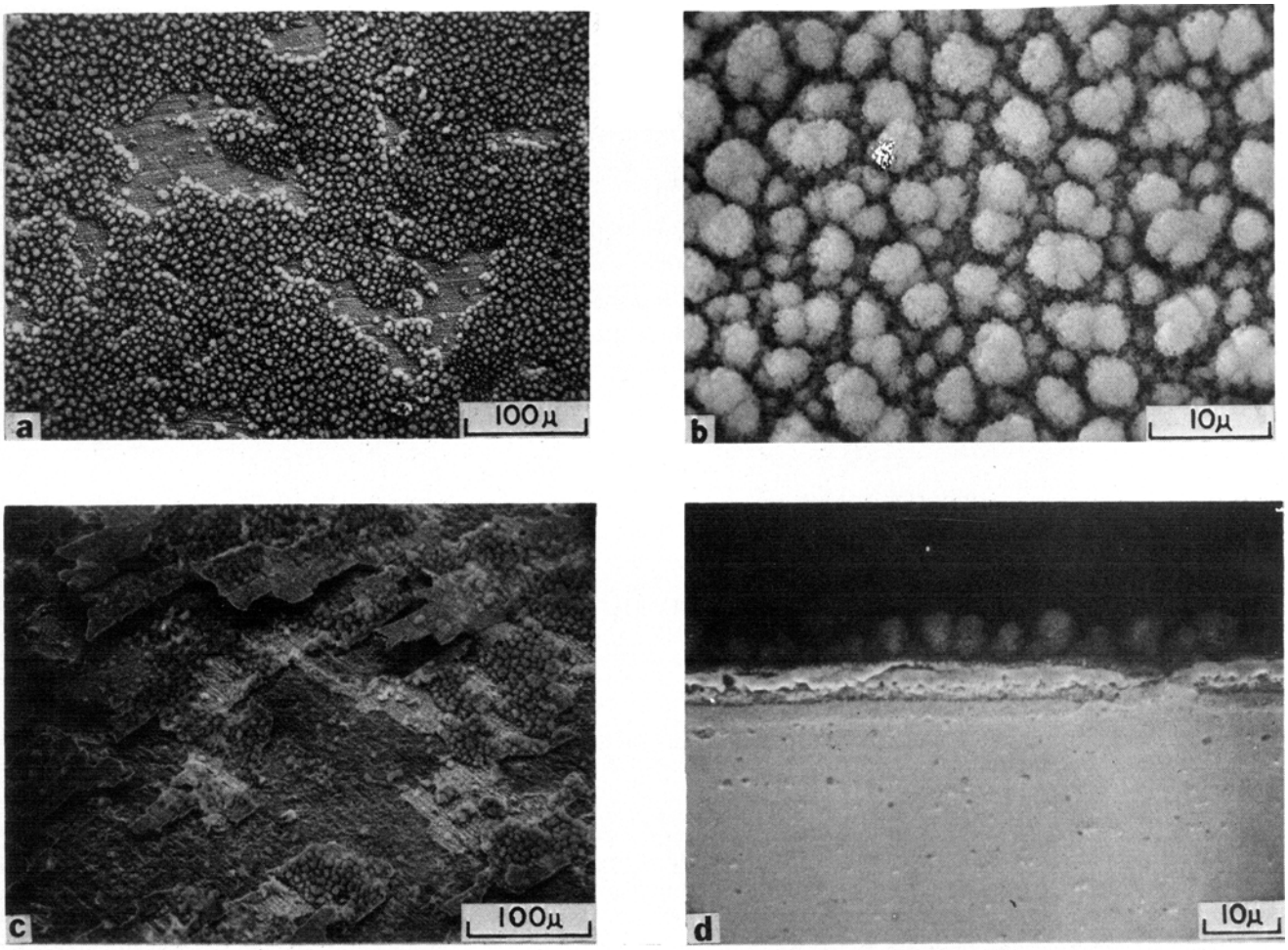

Fig. 4—Surface oxide topography of 1 min exposure specimen. (*a*) showing "mushroom-type" oxide coverage over most of surface, (*b*) higher magnification of typical NiO "mushroom" area, (*c*) showing surface after slightly bending specimen to cause oxide to spall, and (*d*) showing oxide cross-section.

needlelike crystals, typical of crystal growth from condensation processes. The average cluster diameter is of the order of 5 μm. The formation of mushroom type oxide is not uniform over the entire surface, and some regions are seen in Fig. 4(*a*) where the size of the oxide clusters is much smaller than those which cover the majority of the surface. In these regions, the original surface scratches from the prior mechanical polishing are clearly visible. High magnification photographs taken of these areas disclosed that the small mushrooms tended to grow on ridges produced by the belt-sanding pretreatment of the surface and are therefore aligned parallel to the surface scratches. Fig. 4(*c*) was taken of the same specimen after bending slightly to spall part of the surface oxide layer. From this micrograph, it can be seen that the large oxide mushrooms form on top of a solid but friable subscale which is easily fractured and spalled upon bending. Energy dispersive X-ray analysis (EDAX) indicated that the spalled oxide flakes were NiO. No spalling was observed on those regions where small oxide mushrooms formed. EDAX analysis yielded high Cr readings from these areas, suggesting that the small NiO clusters are located on top of a Cr_2O_3 oxide which was very adherent to the alloy substrate. The presence of such a continuous Cr_2O_3 suboxide layer would limit the supply of Ni by separating the surface NiO mushrooms from the underlying alloy, thus explaining why these clusters did not grow as large as those which were in direct contact with an NiO subscale. It would also appear that these small NiO clusters significantly reduce the rate of vaporization of Cr_2O_3 possibly by using up the available atomic oxygen for their own growth. Fig. 4(*d*) is a typical micrograph showing the oxide cross-section of the 1 min exposure specimen from a region where large mushroom clusters were observed. Multiple oxide layers are clearly visible. The surface mushrooms are in contact with a relatively solid outer layer identified to be NiO. The inner oxide layer is separated from the outer NiO by a layer of porous oxide. This porous oxide layer is responsible for the observed weak adherence of the outer NiO which is easily spalled.

Fig. 5 shows, at a higher magnification, the same oxide cross-section as that presented in Fig. 4(*d*). Also shown are four EDAX patterns made by focusing the electron beam to a small spot and positioning the spot at the locations identified on the micrograph. The patterns were made by accumulating counts at each location until the strongest peak reached approximately 95 pct of full scale. No corrections were made on the detected X-ray intensity, consequently, the relative peak height cannot be used directly to read the chemical composition. The horizontal scale on the patterns

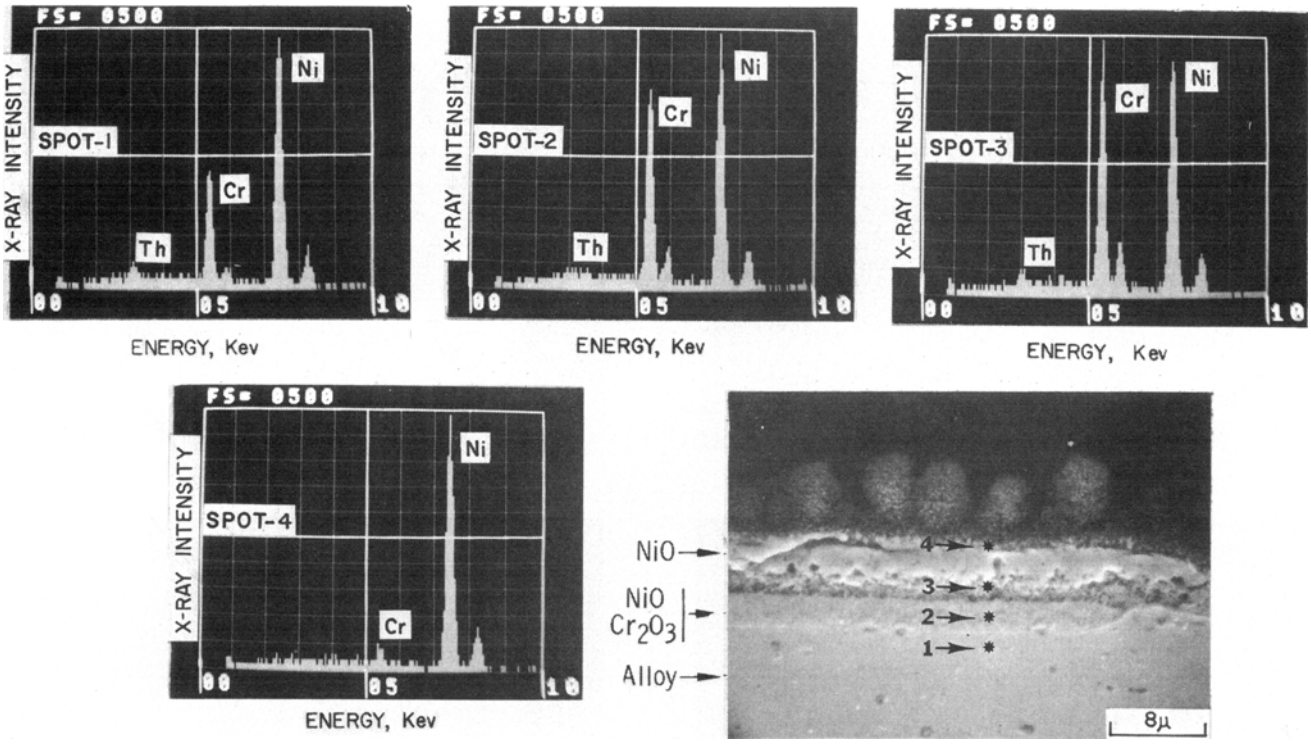

Fig. 5—Oxide cross-section of 1 min exposure specimen and four energy dispersive X-ray (EDAX) patterns taken at the locations marked on the micrograph.

is in the units of keV, thus the X-ray energy characteristic of each peak can be read directly from this scale. The EDAX pattern of spot 1 taken in the alloy, for example, reveals that there are two major peaks present, one located at 5.4 keV and the other at 7.5 keV. These peaks correspond to the K_α lines of Cr and Ni. The small peaks located just to the right of these peaks are the Cr K_β and Ni K_β, respectively. The small peak located at 3.2 keV is the ThM line. The remainder of the spectrum is due to general background. Spot 4 EDAX pattern clearly shows that the subscale on which the mushrooms are attached is NiO. No Th intensity is measurable in this oxide layer, indicating it formed by external growth. Spot 3 and spot 2 patterns were taken of the porous and the inner oxide layers, respectively. The appearance of Th peaks at 3.2 keV in both of these two patterns indicates that these oxide layers grow into the alloy as a result of internal oxidation. In both cases, Ni concentration is lower than that observed in the alloy. It is obvious that Ni ions required for the external growth of NiO come from these oxide layers. The formation of the porous oxide layer is produced by the condensation of vacancies which diffuse inward counter to the flow of Ni ions. No reflections of $NiCr_2O_4$ were identifiably in the X-ray diffraction analysis. Furthermore, microprobe scans showed that the Ni concentration was about twice that of Cr at these two layers. These results suggest that both the porous and the inner oxide layers are a mixture of NiO and Cr_2O_3. There are localized regions where a continuous Cr_2O_3 oxide layer has started to form between the duplex oxide mixture and the alloy substrate. The formation of this inner Cr_2O_3 oxide layer slows the inward growth of the duplex oxide layer. The back surface of the 1 min exposure specimen was also examined. The Cr_2O_3 oxide formed during the static preoxidation treatment was still intact with the alloy with no observable signs of mushroom type oxide formation.

The oxide cross-section of a 10 min exposure specimen along with four EDAX patterns taken at the locations marked on the micrograph are shown in Fig. 6. A comparison of this cross-section with that shown in Fig. 5 reveals that the separate oxide layers just starting to form at 1 min are well developed at 10 min. The oxide scale consists of an outer NiO layer on which the NiO mushrooms are located, an intermediate duplex NiO and Cr_2O_3 layer, and a continuous Cr_2O_3 layer adjacent to the alloy. The previously solid NiO outer layer contains extensive porosity. The Ni intensity from the duplex layer is much lower than the Cr, whereas for the 1 min exposure specimen the two intensities were nearly equal (see Fig. 5, spot-2 and spot-3). These results suggest that Ni has been transported from the oxide subscale to "feed" the surface NiO mushrooms. The mushrooms are more than twice as big as they were on the 1 min exposure specimen. The continuous Cr_2O_3 inner layer appears to isolate the outer oxide scale from any further supply of Ni. The reduced Ni content of the duplex layer and the porosity of the outer NiO layer indicate that the Ni which is transported to the surface is not replenished. Also, since the diffusion of oxygen through Cr_2O_3 is slow, the formation of the continuous inner Cr_2O_3 layer greatly reduced the rate of substrate thickness decrease.

The surface morphology and cross-sections of oxides formed on specimens after 10 min and 30 min of oxidation are shown in Fig. 7. A comparison of these micrographs with those shown in Figs. 3 and 4 clearly indicates that the NiO cluster size increases during the first 30 min. It should, however, be noted that there is little change in cluster size from 10 min to 30 min. The cluster size appears to increase rapidly initially, but

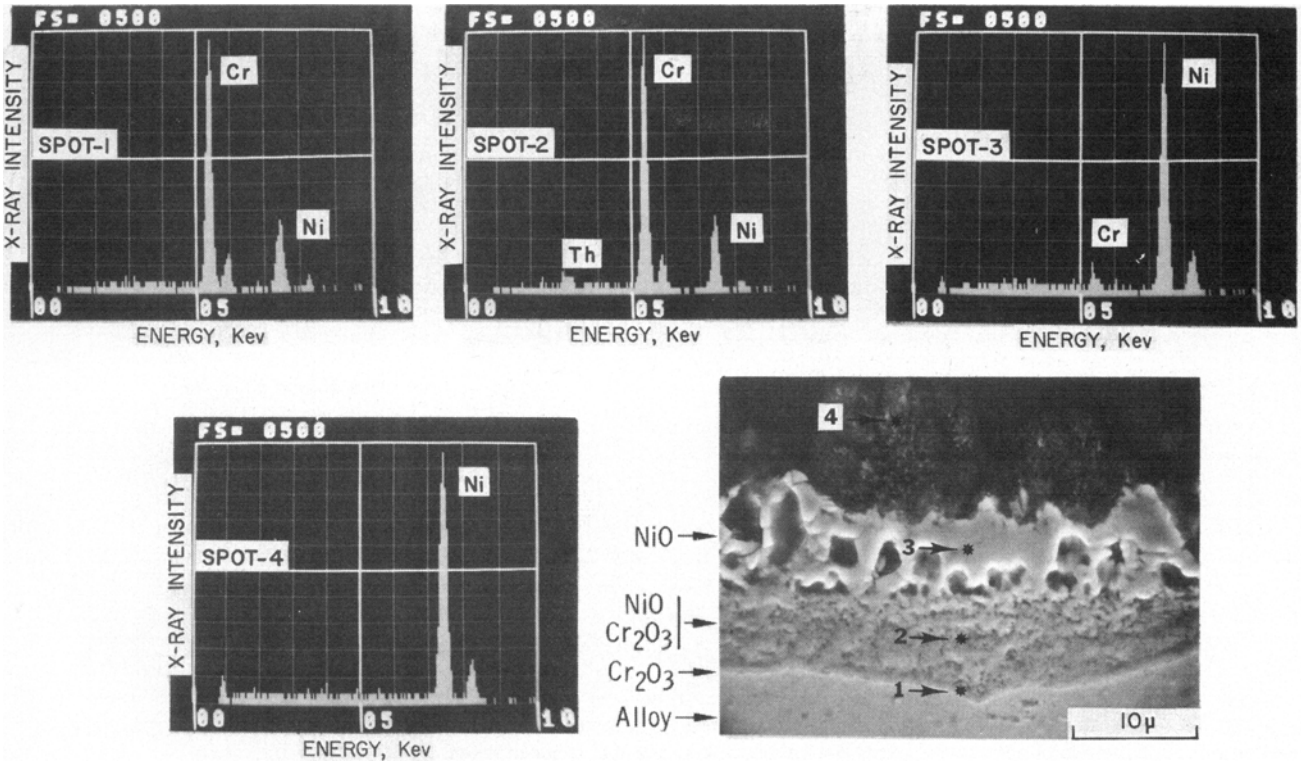

Fig. 6—Oxide cross-section of 10 min exposure specimen and four energy dispersive X-ray (EDAX) patterns taken at the locations marked on the micrograph.

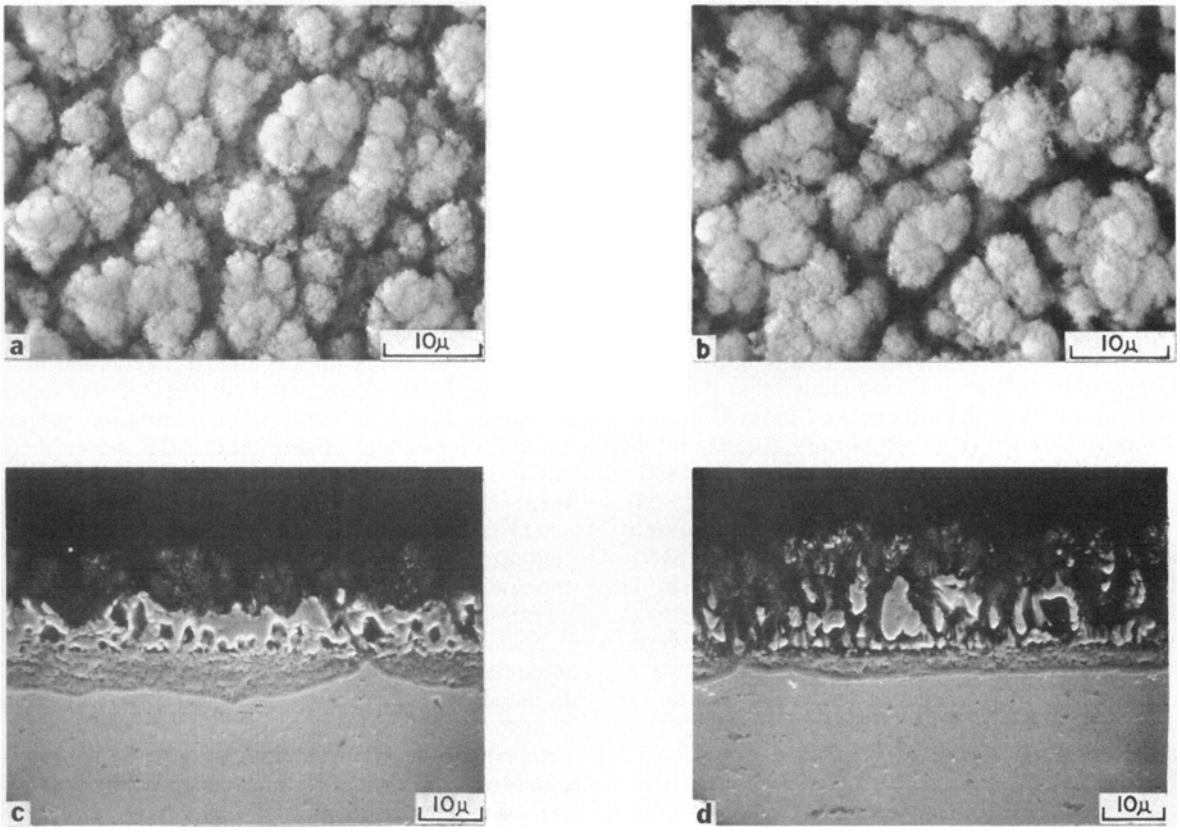

Fig. 7—Typical "mushroom-type" NiO clusters and oxide cross-sections formed on specimens exposed for times of (*a*) 10 min, surface; (*b*) 30 min, surface; (*c*) 10 min, cross-section; and (*d*) 30 min, cross-section.

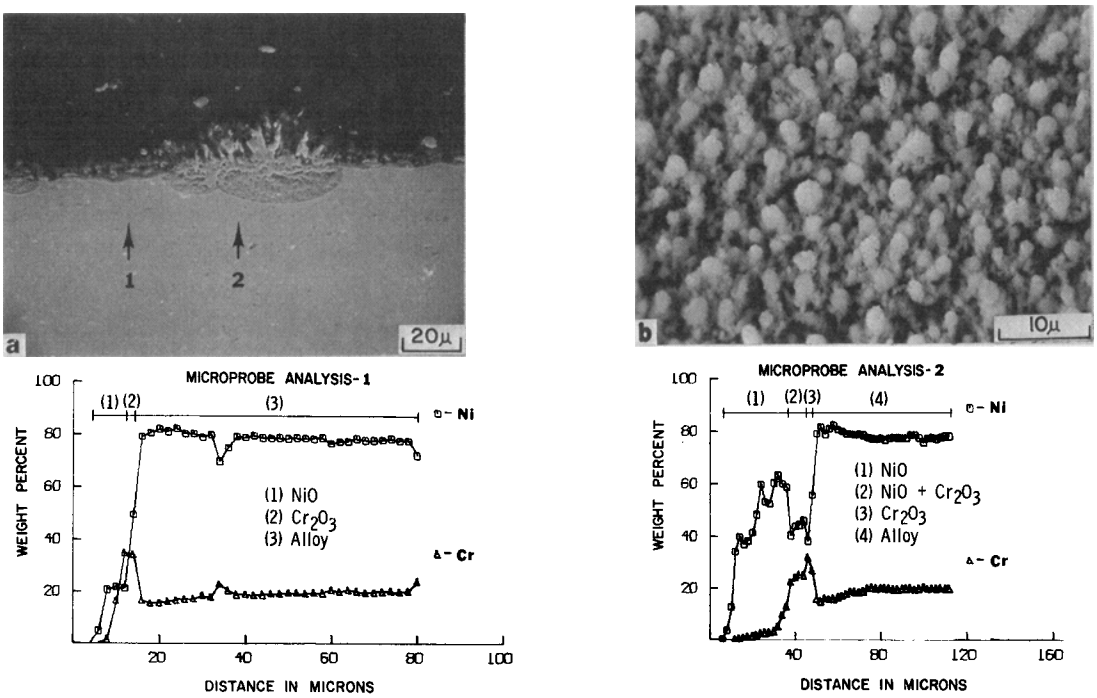

Fig. 8—Micrographs of oxidized surface and cross-section for 2 h exposure specimen and two composition profiles determined by microprobe scans across the oxide cross-section at the locations marked.

grow at a much slower rate once a continuous Cr_2O_3 subscale has developed next to the alloy. This is undoubtedly related to the fact that the Cr_2O_3 layer isolates the NiO-containing surface scale from the alloy thereby requiring that any subsequent supply of Ni to the surface must come from dissociation of part of the NiO in either the duplex layer or the solid outer layer. This apparently is exactly what happens, as evidenced by the development of large cavities in the previously solid NiO layer and the formation of porosity in the duplex layer (see Figs. 7(*c*) and 7(*d*)).

The cavity size in the NiO layer clearly increases from 10 min to 30 min and would be expected to continue to increase with further exposure time. The surface NiO mushrooms remain in contact with the solid segments of this layer which continues to supply the mushrooms with Ni until eventually all the solid NiO segments are used up. Fig. 7 also shows that the thickness of the duplex oxide has decreased from 10 to 30 min, while the inner Cr_2O_3 layer is only slightly thicker. This would seem to indicate that the oxygen released by the dissociation of NiO has been mainly used to oxidize the Cr_2O_3 present in the duplex layer particularly at the regions adjoining the cavities in the outer NiO layer. The CrO_3 vapor thus produced can escape to the atmosphere through the open spaces in the outer scale.

Fig. 8 shows the oxide cross-section and oxide topography of a 2 h exposure specimen. Results of two probe scans made along the lines marked on the micrograph are also given. The mushroom type oxide shown in Fig. 8(*b*) is typical for the 2 h (4-cycles) specimen, and is also typical for those with oxidation times longer than 2 h. The mushroom type oxide clusters are much smaller in size than those observed after 10 to 30 min of exposure. It appears that once the original solid outer NiO layer is totally consumed, the mushroom clusters decrease in size due to vaporization. They are seen to be smoother and more spherical in shape. The oxide cross-section typical at this stage of oxidation is shown in Fig. 8(*a*). There are regions where duplex oxide is no longer observed, and only small fading NiO mushrooms are seen to cover the inner Cr_2O_3 oxide. Microprobe analysis 1 was taken from such a region, as indicated in the cross-sectional micrograph. A slight Cr depleted zone in the alloy is detectable. However, larger Cr depletion is normally observed on probe scans made at similar regions. There are also localized areas where segments of solid NiO are still covering the duplex oxide and large NiO mushrooms are located on top of the NiO segments, a morphology characteristic of that observed at the earlier stages of oxidation. Apparently, localized oxidation occurs at these regions through a new cycle of oxidation following the processes described in the previous sections. Microprobe analysis 2 was taken across a region of local attack. In the duplex oxide the Ni concentration is about double that of Cr. No reflections of $NiCr_2O_4$ were identified in the X-ray diffraction pattern. X-ray diffraction analysis also revealed that the $\{111\}$ alloy reflection was no longer detectable. This indicates that the metal/oxide interface has moved into the specimen to such an extent that the original recrystallized surface layer has been totally oxidized.

Micrographs of oxide cross-section and surface morphology taken from a specimen exposed for 10 h is shown in Fig. 9. Also shown are two composition profiles taken along the lines marked by arrows on the cross-section photograph. The surface mushroom clusters are generally smaller than those found on the two hour exposure specimen (see Fig. 8). As is indicated in Fig. 9(*a*), there are areas of local oxidation where the Cr_2O_3 layer, a duplex oxide mixture, and small porous oxide mushrooms (occasionally large mushroom oxide clusters) are observed. Microprobe

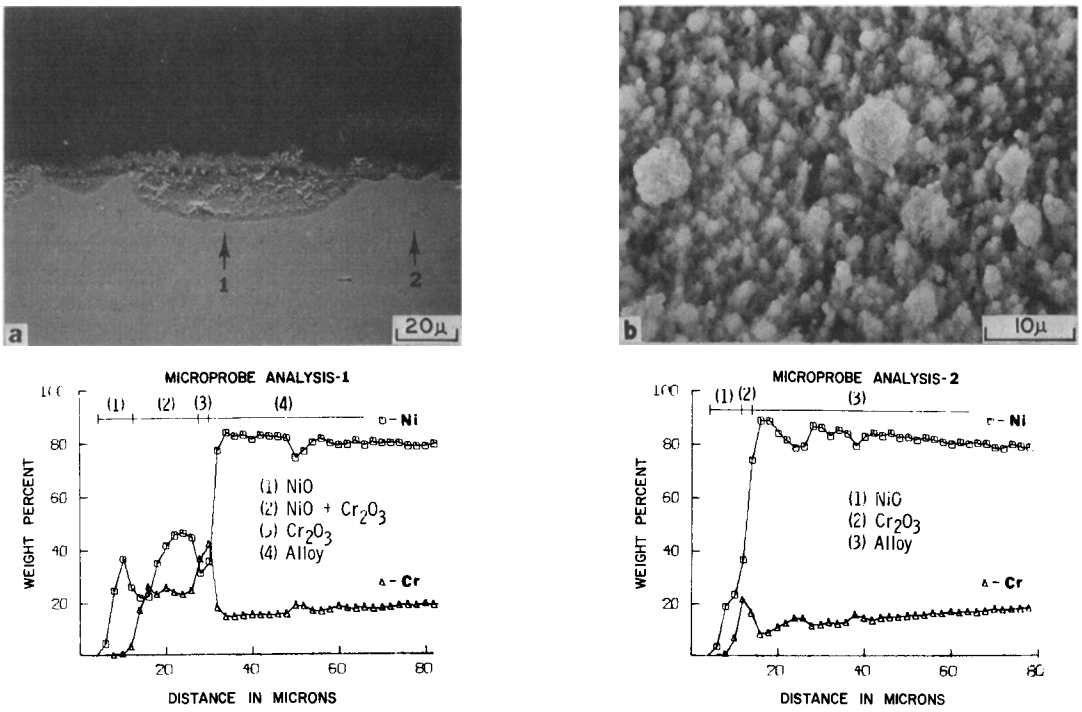

Fig. 9—Micrographs of oxidized surface and cross-section of 10 h exposure specimen and two composition profiles determined by microprobe scans across the oxide cross-section at the locations marked.

analysis 1 reveals that a slight Cr depletion is detected in the alloy substrate. Again, the Ni content is approximately twice that of Cr in the duplex oxide layer. No $NiCr_2O_4$ reflections were identifiable in the X-ray diffraction analysis. There are also regions observed in the figure where duplex oxide has nearly or totally disappeared. The inner Cr_2O_3 layer is not uniform in thickness, being thicker where it is protected by an outer layer of NiO clusters. Apparently, even a porous layer of NiO greatly reduces the rate of vaporization of Cr_2O_3. A rather large Cr depletion zone is persistently observed at these regions, as is seen in microprobe analysis 2. From these observations it appears that, at regions where the Cr depleted alloy is exposed to the air stream, rapid local penetration tends to occur through a new oxidation cycle, thus leading to the appearance illustrated in Figs. 8(*a*) and 9(*a*). Pile-up of ThO_2 particles at the oxide surface was observed from an increase in Th intensity for EDAX patterns taken at the outer edge of duplex oxide layer.

The mushroom type oxide formations were also observed on the back surface of the specimens after 10 or more min of exposure. Without facing directly to the high speed air stream, some of the NiO clusters were able to grow as high as 70 μm. However, the rate of oxidation on the back surface was about 10 times slower than that on the front surface.

Tests were also conducted at 1100°C and 0.002 lbs/sec mass flow rate of the gas. The same general oxidation behavior as that reported above was observed. The mushroom type NiO clusters which formed on the surface were nearly identical in appearance, except that they were generally more dense. The time sequence of the various stages of oxidation discussed above for 1200°C was also different. Work is continuing in an effort to determine how much slower the total

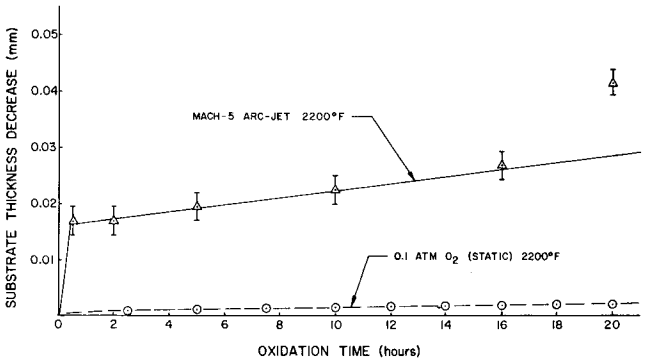

Fig. 10—Substrate thickness decrease of TD-NiCr exposed at 1200°C in a mach-5 arc-jet compared with that calculated from weight gain data for static oxidation in 0.1 atm O_2.

oxidation process proceeded at the lower temperature. Specimens were also tested at 1200°C, using a 0.008 lbs/sec mass flow rate instead of the 0.002 lbs/sec flow rate used for the specimens discussed above. In general, the same basic oxidation behavior was observed for the two different flow rates. The process did proceed somewhat faster at the higher flow rate, but additional samples must be analyzed before a definitive statement is made about the enhancing effect of higher mass flow rates.

To determine the approximate rate of oxidation of the alloy in the dynamic high speed environment, substrate thickness measurements were made before and after arc-jet exposure. The results of these measurements are presented in Fig. 10 and compared with the substrate thickness decrease calculated[33] from weight gain data published for oxidation of TD-NiCr in 0.1 atm of O_2.[3] Substrate thickness decrease in mm is plotted versus oxidation time in h. Initially the specimen undergoes an extremely rapid rate of oxidation

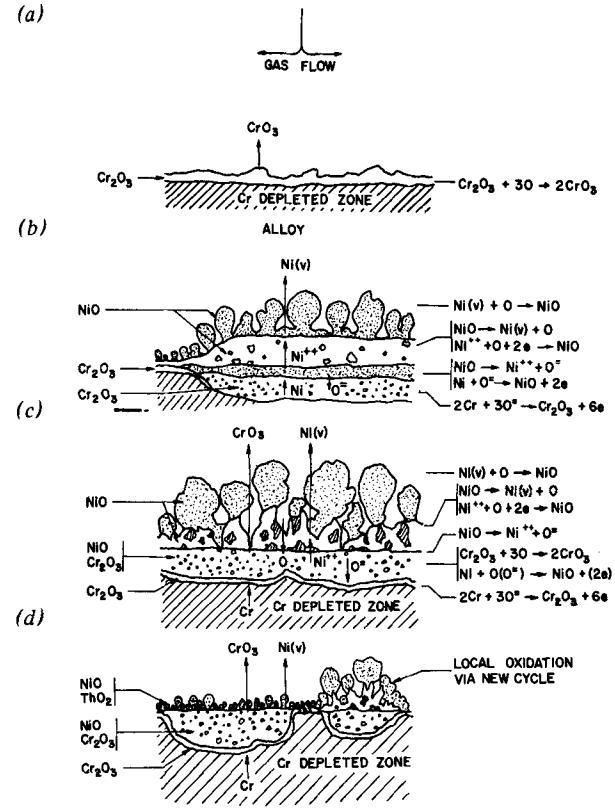

Fig. 11—Schematic diagram of the model for the oxidation of TD-NiCr in a dynamic high-speed flowing air environment containing atomic oxygen. The chronology of oxidation illustrated is divided into four major phases. The essential microstructural features associated with each phase, as well as the important chemical reactions, are shown.

and then oxidizes at a much slowed rate. The shortest time for which substrate thickness decrease measurements were made was 30 min. However, the scanning micrographs taken of the 1 and 10 min exposure specimens suggest that the initial substrate thickness decrease actually took place during the first few minutes of exposure. Had measurements been made for the 10 min exposure specimen it is anticipated that the amount of substrate thickness decrease would have been essentially the same as that measured and reported for the 30 min specimen. It is proposed that the initial loss corresponds to the very rapid rate of oxidation which takes place before a Cr_2O_3 layer has fully developed at the metal/oxide interface. The much slower rate of oxidation measured for longer times is controlled by the rate of vaporization of NiO from the surface.

It will be noted that the amount of alloy oxidized in the dynamic environment is more than an order of magnitude larger than that in the static tests. This is in agreement with previously reported data of Centolanzi,[23] who conducted similar tests on TD-NiCr at 1200°C and found an average metal loss of 0.051 mm after 25 h of exposure. This is approximately 20 times as much metal loss as would be calculated from the static oxidation data used to plot the lower curve in Fig. 10.

Reference to Fig. 10 will show that the amount of metal loss for the 20 h specimen does not fall on the straight line through the other data points. The larger amount of metal loss for this specimen is believed to have been caused by the specimen being accidentally overheated for a few seconds during one of the last few oxidation cycles. This type of overheating occurred only once for this specimen and did not occur for any of the other specimens tested.

DISCUSSION

Based on the observations described above, a model shown in Fig. 11 is postulated to illustrate the dynamic oxidation behavior of TD-NiCr alloy. When the preoxidized specimen is exposed to the mach-5 flowing air environment at 1200°C, the surface Cr_2O_3 oxide is further oxidized to form volatile CrO_3. The atomic oxygen in the air stream, combined with the high speed flow conditions, greatly enhances the oxidation rate, and the approximately 1 μm thick original Cr_2O_3 layer is essentially totally vaporized in 15 sec of exposure. Once the bare alloy is exposed directly to the air stream, both NiO and Cr_2O_3 tend to form on the specimen surface. The NiO, which although not the most favored phase thermodynamically, forms at a much faster rate than Cr_2O_3 and tends to cover most of the surface. The formation of NiO, enhanced[29,30] by the existence of atomic oxygen, proceeds at an extremely fast rate. Reference to Fig. 4 shows that, during the first minute of exposure a solid layer of NiO approximately 4 μm thick is developed on the surface on top of which NiO clusters roughly 4 μm high are located. This rapid outward growth rate strongly suggests that the solid NiO layer is high in Ni^{++} vacancies. While Ni^{++} diffuses through the solid NiO layer and reacts with atomic oxygen at gas/oxide interface, vaporization of NiO is also taking place at the interface. It has been reported[34] that the vaporization of NiO is primarily by dissociation to the elements, *i.e.*, $NiO \rightarrow Ni + O$. It is postulated that a significant fraction of the dissociated Ni vapor will again be oxidized at a latitude above the oxide surface where the concentration of atomic oxygen is relatively high. It is further postulated that part of the NiO thus formed will condense on elevated points on the surface which act as nucleation sites for crystal growth. Ni may also be transported to these sites by surface diffusion and lattice diffusion. The reactions result in a net mass transport of NiO from regions of depression to regions of elevation, leading to the formation of porous mushroom-type oxide clusters. The fact that these oxide clusters form indicates that at this early stage of oxidation (less than 3 min) the rate of NiO condensation is larger than the rate of loss of NiO from the surface of oxide clusters to the gas stream by vaporization. It is also apparent that the rate of outward growth of the solid NiO layer is larger than the rate of evaporation of NiO at the gas/oxide interface. The reactions involved in this stage are shown in Fig. 11(*b*). The rapid development of a duplex layer below the solid NiO layer suggests that at the base of the solid layer the reaction $NiO \rightarrow Ni^{++} + O^{--}$ occurs. Ni^{++} ions diffuse outward to form NiO, and the O^{--} ions diffuse inward and react with the alloy to give a mixture of NiO and Cr_2O_3. The penetration of this internal oxidation will continuously take place until a layer of Cr_2O_3 forms at the oxide/metal interface where the activity of oxygen is reduced to the point where only Cr_2O_3 is formed. The formation of this Cr_2O_3 slows down the inward growth of the duplex oxide layer, and in effect,

isolates the upper oxides from the alloy substrate. The rate of formation of the solid NiO layer which proceeds by mass transport of Ni from the duplex layer is slowed down because the Ni content in the duplex layer is diminishing. As a result of continuous vaporization and condensation, the "mushroom-type" oxide clusters increase in size, while the solid NiO is gradually consumed by continued dissociation and transport of material to the surface oxide clusters. The development of large cavities with NiO "mushrooms" present on the remaining solid segments is typical for the intermediate stage (3 to 30 min) of oxidation. The processes involved are shown in Fig. 11(*c*). On further oxidation (30 min to 2 h) the solid NiO layer is eventually totally consumed by dissociation and transported to the surface. As the supply of Ni to the surface diminishes, the rate of condensation will also be proportionally reduced. When the amount of NiO condensing on the surface becomes less than the amount of NiO being lost to the gas stream by vaporization, the oxide clusters will decrease in size (see Fig. 8(*b*)). The duplex layer becomes rather porous in nature as both Cr_2O_3 and NiO are lost by vaporization. When the duplex layer is totally gone, the inner Cr_2O_3 layer is exposed directly to the airstream. This starts a new oxidation cycle leading to the observed local oxidation regions typical for the later stage of oxidation, Fig. 11(*d*).

The above oxidation sequence is believed to apply to the test conducted at 1100°C as well as the test conducted at 1200°C and 0.008 lbs/sec mass flow rate. The time period of each stage would be expected to vary as the rates of oxidation and vaporization are smaller at 1100°C than at 1200°C. The effect of increasing the mass flow rate should be expected to speed up the oxidation sequence primarily by increasing the available supply of both atomic and molecular oxygen at the specimen surface. An increase in the concentration of atomic oxygen would be expected to be of greater importance than an increase in the concentration of molecular oxygen. The effect of mass flow rate could vary from one stage of oxidation to the next, depending on the rate-controlling mechanism. Mass flow rate would affect the overall time sequence of the oxidation process when the supply of oxygen to the surface was the rate controlling factor.

The effect of atomic oxygen on the oxidation behavior of TD-NiCr at 1100°C in flowing atmospheres has been studied by Gilbreath.[27,28] In atomic oxygen, this alloy was found to have a higher rate of oxide growth, to volatilize faster, and to have greater metal recession than in molecular oxygen. Because of rapid formation of CrO_3, the scale was found to be essentially devoid of chromium, and the emittance of the resulting oxide was reportedly lower than that of oxides formed in molecular oxygen. Gilbreath found that the color of the oxide layer of the specimens tested in a flowing mixture of $O + O_2$ varied from whitish yellow-over-green on the upstream location to gray on the downstream side. The arc-jet specimens tested in this investigation which were whitish or yellow-over-green were always found to have an external NiO mushroom type layer on the surface. Although no SEM micrographs to check oxide morphology were presented, Gilbreath did note that microprobe analysis showed the yellow-over-green area to be nearly all NiO. This suggests that the oxide scale may have been very similar to that observed in this investigation.

SUMMARY AND CONCLUSIONS

The oxidation of TD-NiCr under high temperature high speed flow conditions has been studied and the following results were obtained:

a) The oxidation kinetics of TD-NiCr are controlled by an interplay between the rate of vaporization of NiO and the rate of growth of Cr_2O_3. Although Cr_2O_3 provides good oxidation protection in static environments, it is rapidly lost due to oxidation to gaseous CrO_3 when exposed to the high speed stream containing atomic oxygen. The preferred oxide arrangement for dynamic conditions consists of an outer layer of NiO, an intermediate layer of oxide mixture, and an inner layer of Cr_2O_3. The outer NiO layer reduces the rate of vaporization of the Cr_2O_3 layer and the inner Cr_2O_3 layer restricts the growth rate of the NiO layer.

b) The oxidation process of TD-NiCr was found to be cyclic in nature. The essential steps in this cycle can be summarized as follows:

1) The initial Cr_2O_3 surface oxide is very rapidly lost by formation of gaseous CrO_3.

2) The exposed alloy is oxidized to yield an outer NiO layer, an intermediate duplix oxide, and an inner Cr_2O_3 layer.

3) The inner Cr_2O_3 subscale blocks the supply of Ni to the outer NiO layer with the result that the NiO layer decreases in thickness with time due to continued vaporization.

4) Once the NiO layer is lost, the uncovered Cr_2O_3 layer rapidly vaporizes. However, due to localized differences, this does not occur at the same time over the entire surface.

5) In areas where the alloy is exposed, it again oxidized starting a new cycle.

c) The surface oxide morphology formed under the high speed flow conditions was totally different from that normally observed in static environments. The specimen surfaces were covered with porous NiO clusters having a "mushroom-type" appearance. This type of oxide growth is believed to have been caused by a vaporization and condensation process promoted by the high speed flow conditions in conjunction with the presence of atomic oxygen in the air stream. NiO is susceptible to this type of growth because of its low dissociation energy and rapid reaction with atomic oxygen.

d) The rate of oxidation in the dynamic test conducted was found to be more than an order of magnitude faster than that observed for this alloy in static tests at that same temperature. The rate of substrate thickness decrease measured was comparable to that previously reported for similar tests conducted in other arc-jet apparatus. The results clearly demonstrate that to establish reliability of flight weight heat shields of this alloy, tests must be conducted under simulated re-entry conditions.

CONCLUDING REMARKS

Alloys containing sufficient Al to yield an external layer of Al_2O_3 should be tested because Al_2O_3 would offer significantly better oxidation protection than NiO

or Cr_2O_3. Since Al_2O_3 is an n-type oxide, it should not be adversely affected by the presence of atomic oxygen in the test environment. It is not susceptible to rapid vaporization as is Cr_2O_3. Also, one would not expect it to form surface oxide "mushrooms" as does NiO because it has a much higher dissociation energy. However, the fact that the emissivity of Al_2O_3 is lower than that of either NiO or Cr_2O_3 would be a negative factor when interested in an application such as metallic heat shields for a thermal protection system for space shuttle.

ACKNOWLEDGMENTS

The authors wish to express their gratitude to Mr. Bland Stein, Barry Lisagor, and coworkers at NASA Langley Research Center for their technical advice and assistance in carrying out this research program. The authors would also like to acknowledge Mr. Buford Hunt for the patience and expertise he exercised in making the arc-jet tests. Support of the National Aeronautics and Space Administration, Contract No. NGR-47-0040-082 is gratefully acknowledged.

REFERENCES

1. S. J. Grisaffe and C. E. Lowell: *NASA TN-D-5019*, 1969.
2. C. S. Giggens and F. S. Pettit: *Trans. TMS-AIME*, 1969, vol. 245, pp. 2509-14.
3. C. S. Giggens and F. S. Pettit: *Trans. TMS-AIME*, 1969, vol. 245, pp. 2495-507.
4. C. S. Giggins and F. S. Pettit: *Met. Trans.*, 1971, vol. 2, pp. 1071-78.
5. G. R. Wallwork and A. Z. Hed: *Oxidation of Metals*, 1971, vol. 3, pp. 229-41.
6. H. H. Davis, H. C. Graham, and I. A. Kvernes: *Oxidation of Metals*, 1971, vol. 3, pp. 431-51.
7. J. Stringer, I. G. Wright, B. A. Wilcox, and R. I. Jaffee: Battelle Memorial Inst., Final Report, Naval Air Systems Command Contract No. N00019-71-C-0079, 1971.
8. M. S. Seltzer, J. Stringer, and B. A. Wilcox: Battelle Memorial Inst., Second Quarterly Technical Narrative, NASA Contract No. NAS3-14326, 1971.
9. C. E. Lowell, D. L. Deadmore, S. J. Grisaffe, and J. L. Drell: *NASA TN-D-6290*, 1971.
10. F. J. Kohl and C. A. Stearns: *NASA TMX-52879*, 1970.
11. J. Stringer, B. A. Wilcox, and R. I. Jaffee: *Oxidation of Metals*, 1972, vol. 5, pp. 11-47.
12. J. Stringer: *Oxidation of Metals*, 1972, vol. 5, pp. 49-58.
13. C. E. Lowell: *NASA Technical Memorandum TMX-67867*, 1971.
14. J. Stringer and I. G. Wright: *Oxidation of Metals*, 1972, vol. 5, pp. 59-84.
15. W. L. Hayes: *NASA TMX-64602*, 1971.
16. W. A. Sanders and C. A. Barrett: *NASA TMX-67864*, 1971.
17. C. S. Tedmon, Jr.: *J. Elec. Chem. Soc.*, 1966, vol. 113, pp. 766-68.
18. J. R. Johnston and R. L. Ashbrook: *NASA TN-D 5376*, 1969.
19. H. B. Probst: *NASA SP-227*, 1970, pp. 279-93.
20. W. A. Sanders and H. B. Probst: *NASA TMX-52976*, 1971.
21. H. E. Goldstein: AIAA Paper No. 71-34 presented at AIAA 9th Aerospace Sciences Meeting, New York, New York, Jan. 25-27, 1971.
22. C. E. Lowell and W. A. Sanders: *NASA TN-D-6562*, 1971.
23. F. J. Centolanzi: *NASA TM-X-62015*, 1971.
24. F. J. Centolanzi, H. B. Probst, C. E. Lowell, and N. B. Zimmerman, *NASA TMX-62092*, 1971.
25. "Instructions and Operating Procedures for Aerotherm 100 KW Constrictor Arc Heater System," Aerotherm Corporation, Technical Narrative Report No. IM-68-1, NASA Contract No. NAS1-7560, 1968.
26. J. W. Colby: Magic IV Program, Bell Telephone Laboratories, Inc., 1971.
27. W. P. Gilbreath: *NASA TMX-62064*, 1971.
28. W. P. Gilbreath: *Progress in Astronautics and Aeronautics*, 1972, pp. 127-43.
29. T. D. Tribbeck, J. W. Linnett, and P. G. Dickens: *Trans. Faraday Soc.*, 1969, vol. 65, pp. 890-95.
30. P. G. Dickens, R. Heckingbottom, and J. W. Linnett: *Trans. Faraday Soc.*, 1969, vol. 65, pp. 2235-47.
31. J. W. Schaefer, H. Tong, K. H. Clark, K. E. Suchsland, and G. J. Neuner: NASA CR-AERO Therm Report No. 72-64, Contract No. NAS1-10913, 1973.
32. W. C. Hagel: *J. Amer. Cer. Soc.*, 1965, vol. 48, pp. 70-75.
33. A. V. Pawar: M.S. Thesis, Virginia Polytechnic Institute and State University, 1973.
34. R. T. Grimley, R. P. Burns, and Mark G. Inghram: *J. Chem. Phys.*, 1961, vol. 35, pp. 551-54.